Quantum confinement effects on low-dimensional electron mobility

Tahui Wang, T. H. Hsieh, and T. W. Chen
Department of Electronics Engineering, Institute of Electronics, National Chiao-Tung University, Hsin-Chu, Taiwan, Republic of China

(Received 30 November 1992; accepted for publication 30 March 1993)

A study of quantum confinement effects on the low-dimensional electron mobility in various AlGaAs/GaAs quantum well/wire structures has been performed. The influence of the electron envelop wave function and the subband structure on the low-dimensional electron scattering rates is evaluated. The electron transport behavior is studied through a Monte Carlo simulation. The result shows that the low-dimensional electron mobility varies significantly with the quantum well/wire geometry. The one-dimensional electron mobility of 9200 $cm^2/V\,s$ is obtained in a rectangular quantum wire with a geometry of 110 Å×110 Å. This value is much improved in comparison with the bulk electron mobility of 8000 $cm^2/V\,s$ in intrinsic GaAs and the maximum two-dimensional electron mobility of 8600 $cm^2/V\,s$ in a 120 Å GaAs quantum well. It is also noticed that the highest low-dimensional electron mobility is achieved in a quantum well/wire structure where the energy separation between the first subband and the second subband is about two polar optical phonon energy.

I. INTRODUCTION

The use of low-dimensional electron gas (LDEG) in AlGaAs/GaAs heterostructures to achieve an enhancement of electron mobility has spurred great research interest in recent years. Among the successful demonstrations of the two-dimensional electron gas (2DEG) devices are AlGaAs/GaAs modulation-doped (MOD) field-effect transistors (FETs),[1] AlGaAs/InGaAs/GaAs pseudomorphic MODFETs,[2] multiple quantum well FETs,[3] and GaAs gate heterojunction FETs.[4] More recently, various advanced quantum-wire structures have been invented to realize the speed advantage of one-dimensional electron gas (1DEG).[5–7] Both experimental and theoretical studies have shown the possibility that the mobilities of the low-dimensional electron gases can be greatly improved due to the quantum confinement effects.[5,8]

Since the electron scattering rate is closely related to an electron wave function distribution and a subband structure, the LDEG mobility may change significantly with the shape of quantum wells/wires. In this article, we investigate the quantum structure geometrical effects on the LDEG mobility by tailoring the subband structure and the electron wave function. The mobilities of 1DEG, 2DEG, and bulk electrons will be compared.

Two methods are usually employed to analyze the low-dimensional electron transport properties in the subbands of quantum wells/wires. One is to solve the Boltzmann transport equation directly[9] and the other is to use a Monte Carlo method.[10] Since the traveling wave vectors of the LDEG are confined to a one-dimensional space (1DEG) or to a two-dimensional space (2DEG), the computational time needed to find an electron final state after a scattering is largely reduced in a Monte Carlo simulation. This is especially true for the 1DEG case because only two possible final states, forward or backward, are involved. Currently, it becomes more popular to use the Monte Carlo method to explore the LDEG transport physics.

The major scattering mechanisms in GaAs at a low electric field include polar optical phonon (POP) scattering, acoustic phonon (ACP) scattering, and ionized impurity scattering. POP scattering is a dominant process if the concentration of the ionized impurity atoms are comparatively less in materials such as intrinsic GaAs. The effect of ionized impurity scattering can therefore be ignored in some device configurations. As far as the low-field mobility is concerned in this work, electron transport in the satellite valleys (L and X valleys) is also neglected since the vast majority of conducting electrons reside in the Γ valley.

II. LDEG TRANSPORT MODEL

Two sorts of 2DEG quantum-well structures and rectangular 1DEG quantum-wire structures are studied. Electron concentrations in these devices are sufficiently low to maintain the nondegenerate condition. The subband structure and the electron wave function in the quantum wells/wires are obtained by solving the Schrödinger equation under an effective mass approximation. The 2DEG and the 1DEG wave functions are expressed below:

$$\psi_{2D}=\frac{1}{\sqrt{A}}\exp(ik_{\parallel}\,r_{\parallel}\,)\varphi(z), \tag{1a}$$

$$\psi_{1D}=\frac{1}{\sqrt{L_x}}\exp(ik_x x)\varphi(y,z), \tag{1b}$$

where φ represents an electron envelop wave function in the quantization direction, A is the area of a quantum well, $k_{\parallel}$ is the electron wave vector component parallel to the quantum well, and L_x is the length of a quantum wire. The quantization is in the z direction for the 2DEG and in both the y and z directions for the 1DEG.

Using the wave functions in Eqs. (1a) and (1b), we obtain the square of the matrix elements between the mth and the nth subbands:

 0021-8979/93/74(1)/426/5/$6.00

$$|M_{mn}|^2_{2D}=\left(\frac{1}{2\pi}\right)\int |M_{3D}(q_x,q_y,q_z)|^2 \times |I_{mn,2D}(q_z)|^2 dq_z, \quad (2a)$$

$$|M_{mn}|^2_{1D}=\left(\frac{1}{2\pi}\right)^2\iint |M_{3D}(q_x,q_y,q_z)|^2 \times |I_{mn,1D}(q_y,q_z)|^2 dq_y dq_z, \quad (2b)$$

where M_{3D} is the corresponding matrix element for a bulk electron and q is a phonon wave vector. The overlap integral I_{mn} in the above equations is defined as

$$I_{mn,2D}(q_z)=\int \varphi_m(z)\varphi_n(z)\exp(iq_z z)dz, \quad (3a)$$

$$I_{mn,1D}(q_y,q_z)=\iint \varphi_m(y,z)\varphi_n(y,z) \times \exp(iq_y y)\exp(iq_z z)dydz. \quad (3b)$$

Accordingly, the coupling coefficient for the 2DEG was derived in Ref. 11:

$$H_{mn,2D}(q_\parallel)=\iint dz_1 dz_2 \varphi_m(z_1)\varphi_n(z_1)\varphi_m(z_2)\varphi_n(z_2) \times \exp(-q_\parallel |z_2-z_1|), \quad (4a)$$

and the 1DEG coupling coefficient is derived in the Appendix:

$$H_{mn,1D}(q_x)=\iiint dy_1 dy_2 dz_1 dz_2 \varphi_m(y_1,z_1) \times \varphi_n(y_1,z_1)\varphi_m(y_2,z_2)\varphi_n(y_2,z_2) \times 2K_0(q_x\sqrt{|y_2-y_1|^2+|z_2-z_1|^2}), \quad (4b)$$

where $q_\parallel$ is the phonon wave vector component parallel to the quantum well and K_0 is the modified Bessel function of the second kind of order 0. Using the matrix elements, the 2DEG and 1DEG POP scattering rates are readily obtained in the following:

$$S^{pop}_{mn,2D}(E)=\frac{e^2 w}{8\pi\epsilon_0}\left(\frac{1}{\epsilon_\infty}-\frac{1}{\epsilon_s}\right)\left(N_w+\frac{1}{2}\pm\frac{1}{2}\right) \times \int \frac{H_{mn,2D}(q_\parallel)}{q_\parallel}\delta(k'_\parallel-k_\parallel\pm q_\parallel) \times \delta(E'-E\pm\hbar w)dk'_\parallel, \quad (5a)$$

$$S^{pop}_{mn,1D}(E)=\frac{e^2 w}{8\pi\epsilon_0}\left(\frac{1}{\epsilon_\infty}-\frac{1}{\epsilon_s}\right)\left(N_w+\frac{1}{2}\pm\frac{1}{2}\right) \times \int H_{mn,1D}(q_x)\delta(k'_x-k_x\pm q_x) \times \delta(E'-E\pm\hbar w)dk'_x, \quad (5b)$$

with

$$N_w=\frac{1}{\exp(\hbar w/k_B T)-1}.$$

Here ϵ_∞ and ϵ_s are optical and static dielectric constants, N_w is the phonon occupation number, and $\hbar w$ is polar optical phonon energy. The values used for ϵ_∞ and ϵ_s are 10.92 and 12.90, respectively, $\hbar w$ is chosen to be 35.4 meV and the temperature T is 300 K. The $\pm$ signs stand for phonon emission and absorption, respectively. E' and E denote initial-state and final-state electron energies.

Acoustic-phonon scattering for the LDEG is treated similarly to polar optical phonon scattering. The 2DEG and the 1DEG ACP scattering rates are given by

$$S^{acp}_{mn,2D}(E)=\frac{m^* k_B T D_A^2}{\hbar^3 \rho S_l^2}\int \varphi_m^2(z)\varphi_n^2(z)dz, \quad (6a)$$

$$S^{acp}_{mn,1D}(E)=\frac{k_B T D_A^2}{\hbar\rho S_l^2}\iint \varphi_m^2(y,z)\varphi_n^2(y,z)g_{1D}(E)dydz. \quad (6b)$$

The GaAs material parameters used in the calculation are deformation potential $D_A=7.0$ eV, the density of mass $\rho=5.36$ g/cm^3, and longitudinal sound velocity $S_l=5.24\times10^5$ cm/s. $g_{1D}(E)$ is the density of states for the 1DEG with a broadening factor of 2.5 meV at 300 K.[12]

In the Monte Carlo simulation, a single electron is simulated under an external electric field. It travels freely between two successive scatterings. The free-flight time is determined by a random number and by the total scattering rate evaluated above. During the free flight, the electron is accelerated by the field and its momentum and energy are updated. If a scattering happens, another random number is generated to decide the responsible scattering mechanism and the new electron state is chosen according to the subband structure. We continue this procedure until the fluctuation in mobility due to the statistical uncertainty is less than 0.5%. Usually, it needs about 5 000 000 scattering events for an electric field smaller than 1 kV/cm.

III. RESULTS AND DISCUSSION

The LDEG scattering rate can be modulated with respect to the bulk electron scattering rate in two aspects; the overlap integral and the density of states. As the size of a quantum well/wire increases, the intrasubband scattering

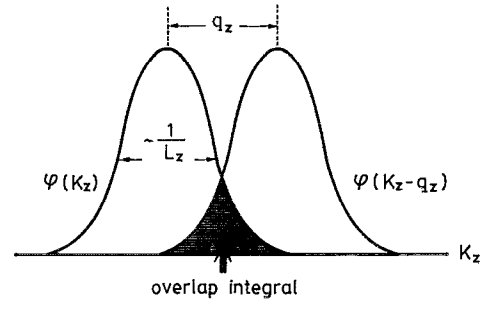

FIG. 1. Illustration of the overlap integral [Eq. 3(a)] of an intrasubband scattering. q_z is the phonon wave vector in the quantized direction and φ is an electron wave function in momentum space. L_z is the quantum well width. The shaded area represents the overlap integral.

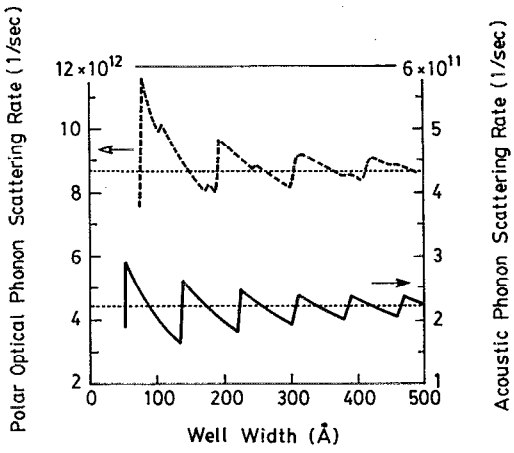

FIG. 2. POP and ACP scattering rates vs a quantum well width at an electron energy of 80 meV. The solid line is the 2DEG ACP scattering rate, the dashed line is the 2DEG POP scattering rate and the dotted lines represent the bulk electron scattering rates. $T=300$ K.

rate is lowered due to the spread of an electron envelop wave function. This can be understood from the illustration of Fig. 1. The spread of the 2DEG wave function in coordinate space transforms into a narrower distribution in momentum space due to the uncertainty principle. For a fixed phonon momentum in the quantized direction q_z, only the shaded region in Fig. 1 contributes to the overlap integral [Eq. (3a)]. A sharp distribution in momentum space results in a smaller overlap region and thus a smaller scattering rate. Therefore, the 2DEG scattering rate declines with a well width until at a certain width the electron transition to the next subband takes place. The sawtooth-like feature of the 2DEG scattering rates in a $Al_{0.3}Ga_{0.7}As/GaAs/Al_{0.3}Ga_{0.7}As$ quantum well is shown in Fig. 2. The result reveals that there exists a window of a well width in which the 2DEG scattering rate can be minimized. This suggests that an optimization of the electron mobility is achievable in certain geometry quantum structures.

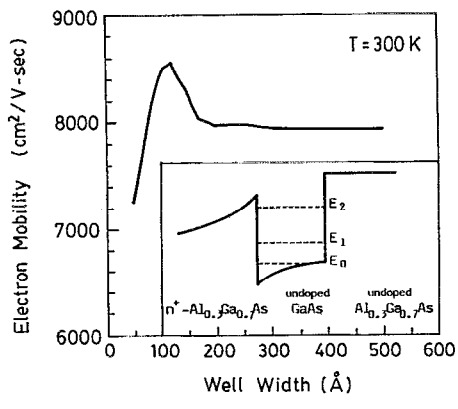

FIG. 3. Calculated 2DEG mobility as a function of a well width. The inset of the figure shows the conduction band edge and the quantum states.

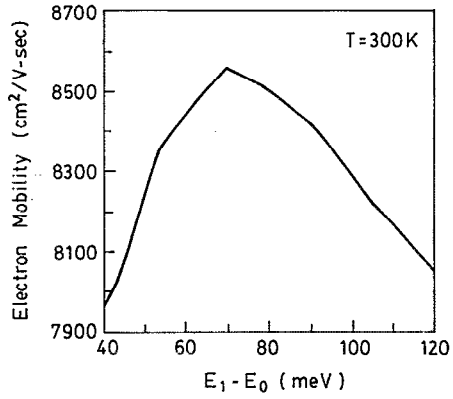

FIG. 4. 2DEG mobility vs the energy difference between the first subband and the second subband at 300 K.

Two sorts of the 2DEG quantum-well structures are studied at $T=300$ K. The first kind has a 500 Å n^+ $Al_{0.3}Ga_{0.7}As/30$ Å i-$Al_{0.3}Ga_{0.7}As/GaAs/i$-$Al_{0.3}Ga_{0.7}As$ quantum well. The doping concentration in the n^+ AlGaAs layer is 1×10^{18} 1/cm^3. A 30 Å undoped spacer is included. The GaAs well width is varied in the simulation. The second kind structures have a n^+ GaAs gate/i-$Al_{0.4}Ga_{0.6}As/i$-GaAs configuration.[4] The quantum well has a triangle-like geometry at the AlGaAs/GaAs interface. In the latter structures, the interface field is varied to adjust the subband structure and the spread of the electron wave function. In the simulation, the Schrödinger and the Poisson equations are solved self-consistently.

Figure 3 shows the 2DEG mobility as a function of a well width in the first kind of quantum wells. The self-consistent conduction band-edge diagram and the subband structure are plotted in the inset of the figure. The peak mobility of about 8600 cm^2/V s is obtained at a width of 120 Å. In Fig. 4, we redraw the 2DEG mobility against the energy difference between the first subband (E_0) and the second subband (E_1). A maximum mobility around $E_1-E_0=2\hbar w$ is noticed. In order to explain this result, we calculate the electron distribution functions in a 120 Å well at fields of 1.0 and 2.0 kV/cm in Fig. 5. The equilibrium

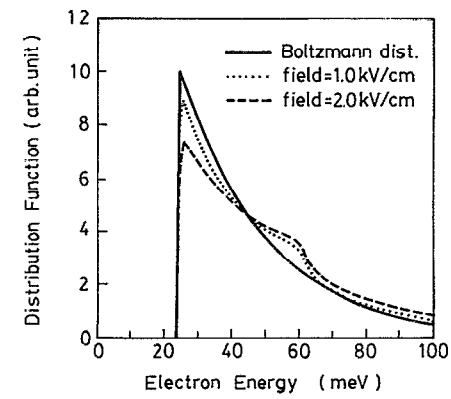

FIG. 5. The electron distributions plotted as a function of electron energy. The solid line represents the equilibrium Boltzmann distribution.

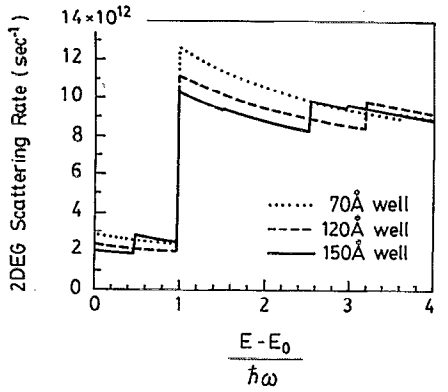

FIG. 6. The 2DEG scattering rates plotted as functions of electron energy in 70, 120, and 150 Å quantum wells.

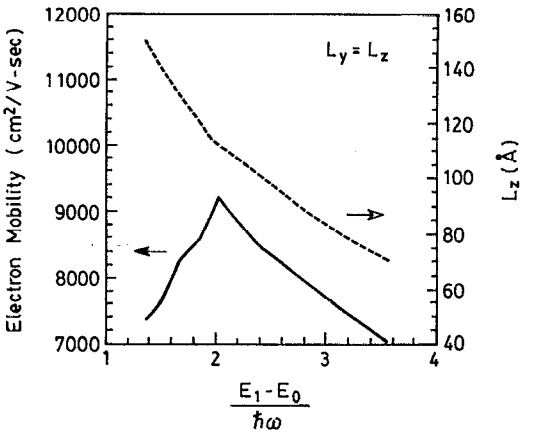

FIG. 8. Dependence of the 1DEG mobility on the quantum-wire size and the energy separation between the lowest two subbands. $\hbar w$ is polar optical phonon energy.

Boltzmann distribution is shown as a reference. The deviation of the distribution functions from the equilibrium Boltzmann distribution under an applied field is due to field acceleration. The significant drop about $1\hbar w$ above the ground state in Fig. 5 is due to the POP emission. In other words, the majority of the electrons are restricted in the energy range from E_0 to $E_0+\hbar w$ due to the POP emission. The corresponding 2DEG scattering rates in 70, 120, and 150 Å quantum wells as functions of electron energy are plotted in Fig. 6. In the 70 Å quantum well where the subband structure has $E_1-E_0>2\hbar w$, although the majority of the electrons are virtually immune from intersubband scattering, the electrons have the largest intrasubband scattering rate as shown in Fig. 6. On the other hand, when $E_1-E_0<2\hbar w$ (for example, the 150 Å well), the majority of the first subband electrons suffer from serious intersubband scattering. Therefore, the 2DEG has a peak mobility around $E_1-E_0=2\hbar w$.

In the second kind of the quantum-well structures, the 2DEG mobility versus the energy separation between E_1 and E_0 is shown in Fig. 7. The triangle-like quantum well geometry with the subband structure is illustrated in the inset of Fig. 7. A similar result of a peak mobility at $E_1-E_0=2\hbar w$ is observed. However, the peak mobility (8250 cm^2/V s) in the triangle-like quantum well is somewhat lower than that (8600 cm^2/V s) in the rectangle-like quantum well.

The 1DEG quantum wire structure in this work is designed to have intrinsic GaAs embedded in a rectangular area ($L_y\times L_z$) confined by $Al_{0.3}Ga_{0.7}As$. Figure 8 shows the 1DEG mobility as a function of L_z. The result indicates that the highest mobility of 9200 cm^2/V s is obtained in a 110 Å×110 Å quantum wire. This value is greater than the maximum 2DEG mobility of 8600 cm^2/V s and the bulk electron mobility of 8000 cm^2/V s in intrinsic GaAs. It should be pointed out that the occurrence of the mobility peak at $E_1-E_0=2\hbar w$ in Fig. 8 is even clearer in a quantum wire. The reason is that the 1DEG distribution function has a steeper drop at $E_0+\hbar w$ due to the enhanced POP emission. The scattering rates of 1DEG, 2DEG, and bulk electrons are shown in Fig. 9 for a comparison. Apparently, the 1DEG scattering rate has a largest POP emission rate at $E=E_0+\hbar w$ arising from the singularity of the 1DEG density of states.

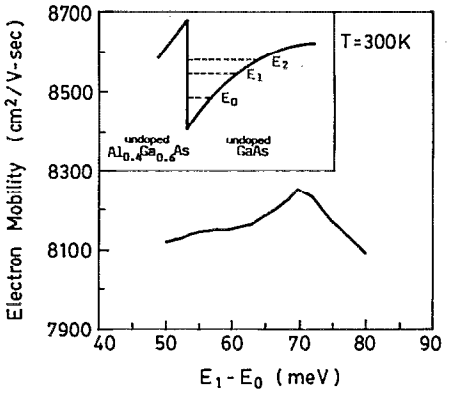

FIG. 7. 2DEG mobility vs the energy separation between E_1 and E_0 in the triangular quantum wells. The inset illustrates the conduction band-edge profile and the subband structure.

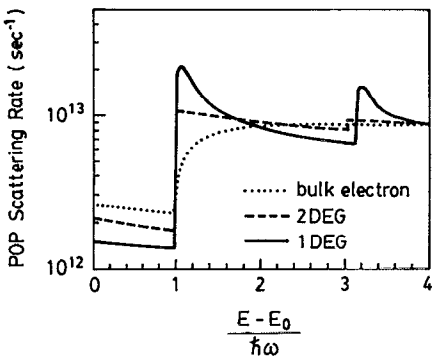

FIG. 9. Comparison of the POP scattering rates of 1DEG, 2DEG, and bulk electrons. The 2DEG structure has a 120 Å well width and the 1DEG structure has a 110 Å×110 Å geometry.

IV. CONCLUSIONS

As a conclusion, our study indicates that the 2DEG mobility varies significantly with the quantum well geometry from 7250 cm^2/V s in a 50 Å rectangular well to 8600 cm^2/V s in a 120 Å rectangular well. The 1DEG mobility varies from 7050 cm^2/V s in a 70 Å×70 Å wire to 9200 cm^2/V s in a 110 Å×110 Å wire. The maximum mobility of the LDEG is found in a quantum structure where the energy difference between the first subband and the second subband is about $2\hbar w$, or 70 meV in GaAs.

ACKNOWLEDGMENT

Financial support from National Science Council, R.O.C., under Contract No. NSC82-0404-E-009-128 is greatly acknowledged.

APPENDIX

The square of the matrix element between the mth subband and the nth subband for the 1DEG is evaluated below:

$$|M_{mn}|^2_{1D}=\left(\frac{1}{2\pi}\right)^2\int\int dq_y dq_z |M_{3D}(q_x,q_y,q_z)|^2 |I_{mn,1D}(q_y,q_z)|^2$$
$$=\left(\frac{1}{2\pi}\right)^2\int\int dq_y dq_z \frac{e^2\hbar w}{2\epsilon_0}\left(\frac{1}{\epsilon_\infty}-\frac{1}{\epsilon_s}\right)\frac{1}{q_x^2+q_y^2+q_z^2}\int\int\int dy_1 dy_2 dz_1 dz_2[\varphi_{mn}(y_1,z_1)\varphi_{mn}(y_2,z_2)$$
$$\times\exp(-iq_y|y_2-y_1|)\exp(-iq_z|z_2-z_1|)], \tag{A1}$$

where $\varphi_{mn}(y,z)=\varphi_m(y,z)\varphi_n(y,z)$.

The coupling coefficient is defined as follows:

$$H_{mn,1D}(q_x)=\frac{1}{\pi}\int\int\int dy_1 dy_2 dz_1 dz_2 \varphi_{mn}(y_1,z_1)$$
$$\times\varphi_{mn}(y_2,z_2)\int\int dq_y dq_z \frac{1}{q_x^2+q_y^2+q_z^2}$$
$$\times\exp(-iq_y|y_2-y_1|)\exp(-iq_z|z_2-z_1|). \tag{A2}$$

Using a multiple Fourier transform over q_y and q_z,[13] we have

$$\int\int dq_y dq_z \frac{1}{q_x^2+q_y^2+q_z^2}\exp(-iq_y|y_2-y_1|)$$
$$\times\exp(-iq_z|z_2-z_1|)$$
$$=2\pi K_0(q_x\sqrt{|y_2-y_1|^2+|z_2-z_1|^2}) \tag{A3}$$

and

$$H_{mn,1D}(q_x)=\int\int\int\int dy_1 dy_2 dz_1 dz_2 \varphi_{mn}(y_1,z_1)$$
$$\times\varphi_{mn}(y_2,z_2)2K_0(q_x\sqrt{|y_2-y_1|^2+|z_2-z_1|^2}). \tag{A4}$$

From the Fermi–Golden rule, the scattering rate is then obtained:

$$S^{pop}_{mn,1D}(E)=\frac{e^2 w}{8\pi\epsilon_0}\left(\frac{1}{\epsilon_\infty}-\frac{1}{\epsilon_s}\right)\left(N_w+\frac{1}{2}\pm\frac{1}{2}\right)$$
$$\times\int H_{mn,1D}(q_x)\delta(k'_x-k_x\pm q_x)$$
$$\times\delta(E'-E\pm\hbar w)dk'_x. \tag{A5}$$

[1] T. Mimura, S. Hiyamizu, T. Fujii, and K. Nanbu, Jpn J. Appl. Phys. **19**, L225 (1980).
[2] L. Nguyen, W. Schaff, P. Tasker, A. Lepore, L. Palmateer, M. Foisy, and L. Eastman, IEEE Trans. Electron Device **ED-35**, 139 (1988).
[3] N. Sheng, C. P. Lee, R. T. Chen, D. Miller, and S. J. Lee, IEEE Electron. Device Lett. **EDL-6**, 3078 (1985).
[4] P. M. Solomon, C. M. Knoedler, and S. L. Wright, presented at IEEE Device Res. Conf. 1984.
[5] S. Nakata, S. Yamada, Y. Hirayama, T. Saku, and Y. Norikoshi, Jpn. J. Appl. Phys. **29**, 48 (1990).
[6] Y. Nakamura, S. Koshiba, M. Tsuchiya, H. Kano, and H. Sakaki, Appl. Phys. Lett. **59**, 700 (1991).
[7] S. Tsukamoto, Y. Nagamune, M. Nishioka, and Y. Arakawa, J. Appl. Phys. **71**, 533 (1992).
[8] H. Sakaki, Jpn. J. Appl. Phys. **19**, L735 (1980).
[9] T. Yamada and J. Sone, Phys. Rev. B **40**, 6265 (1985).
[10] S. Briggs and J. P. Leburton, Phys. Rev. B **38**, 8163 (1988).
[11] B. K. Ridley, J. Phys. C **15**, 5899 (1982).
[12] S. Briggs and J. P. Leburton, Phys. Rev. B **43**, 4785 (1991).
[13] F. Oberhettinger, *Tables of Fourier Transforms and Fourier Transforms of Distributions* (Springer, Berlin, 1990).